JCTC Journal of Chemical Theory and Computation

Article

pubs.acs.org/JCTC

Concerted Cyclization of Lanosterol C-Ring and D-Ring Under Human Oxidosqualene Cyclase Catalysis: An ab Initio QM/MM MD Study

Nanhao Chen,[†] Jingwei Zhou,[†] Jiabo Li,[‡] Jun Xu,[†,*] and Ruibo Wu[†,*]

[†]School of Pharmaceutical Sciences, Sun Yat-sen University, Guangzhou 510006, P.R. China

[‡]Schrödinger, LLC., 120 West 45th Street, 17th Floor, New York, New York, 10036 United States

Supporting Information

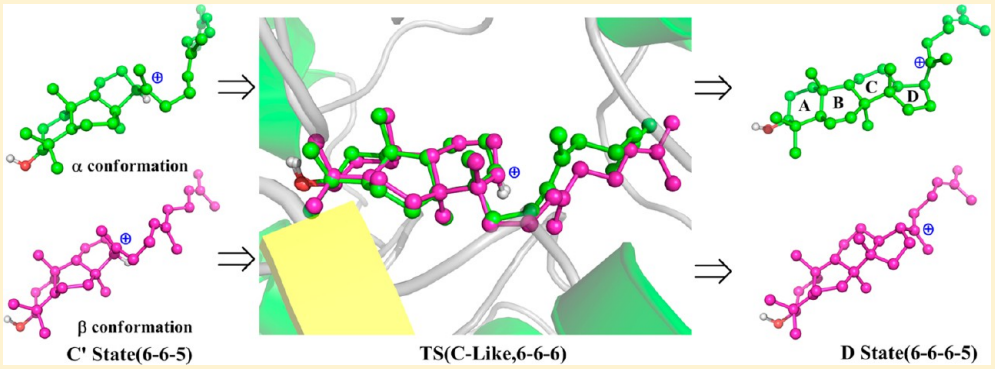

ABSTRACT: Human oxidosqualene cyclase (OSC) is one key enzyme in the biosynthesis of cholesterol. It can catalyze the linear-chain 2,3-oxidosqualene to form lanosterol, the tetracyclic (6−6−6−5 members for A−B−C−D rings) cholesterol precursor. It also has been treated as a novel antihyperlipidemia target. In addition, the structural diversity of cyclic terpenes in plants originates from the cyclization of 2,3-oxidosqualene. The enzyme catalytic mechanism is considered to be one of the most complicated ones in nature, and there are a lot of controversies about the mechanism in the past half a century. Herein, state-of-the-art ab initio QM/MM MD simulations are employed to investigate the detailed cyclization mechanism of C-ring and D-ring formation. Our study reveals that the C and D rings are formed near-synchronously from a stable "6−6−5" ring intermediate. Interestingly, the transition state of this concerted reaction presents a "6−6-6" structure motif, while this unstable "6−6-6" structure in our simulations is thought to be a stable intermediate state in most previous hypothetical mechanisms. Furthermore, as the tailed side chain of 2,3-oxidosqualene shows a β conformation while it is α conformation in lanosterol, finally, it is observed that the rotatable "tail" chain prefers to transfer β conformation to α conformation at the "6−6−5" intermediate state.

INTRODUCTION

As early as 1965, the elucidation and characterization of cholesterol biosynthesis had been clarified by Konrad.[1] As one of the products of the mevalonate pathway (MVP),[2,3] cholesterol has many functions in human beings.[4−8] However, excess cholesterol leads to hypercholesterolemia, which ultimately leads to atherosclerosis and stroke. Now, hyperlipidemia is thought to be one of the most dangerous and high-incidence diseases in developed countries.[9,10] So in the last century, many large pharmaceutical companies invested a lot on hypolipidemic, and now statin drugs are one of the best-selling cholesterol-lowing drugs.[11,12] Lipitor, the most famous statin drug, has topped the list of best-selling branded pharmaceuticals in the world for nearly a decade.[13] As the target of the statin drugs, hydroxymethylglutaryl-coenzyme A (HMG-CoA) reductase is the best-known hypolipidemic target.[14] As seen from the brief MVP (shown in Figure 1), HMG-CoA reductase is located upstream of the pathway and its inhibitors can reduce the synthesis of cholesterol. However, the inhibition of HMG-CoA reductase can also reduce the level of nonsterol intermediates synthesized and lead to the decrease of "second messenger".[15,16] Moreover, statin drugs cannot reduce the plasma low-density lipoprotein (LDL)-cholesterol concentration which is the recommended clinical treatment objective in hypolipidemic therapy.[12] Therefore, the oxidosqualene cyclase (OSC), which functions downstream of squalene in the MVP, attracts more and more attention as a novel hypolipidemic target in recent years.[17−20] Therefore, a deep understanding of the enzyme catalytic mechanism of OSC is important for the inhibitor design.

As shown in Figure 1, the human OSC (also namely lanosterol synthesis, LAS), catalyzes the 2,3-oxidosqualene to form lanosterol via cyclization (to yield a key intermediate:

Received: October 30, 2013
Published: January 24, 2014

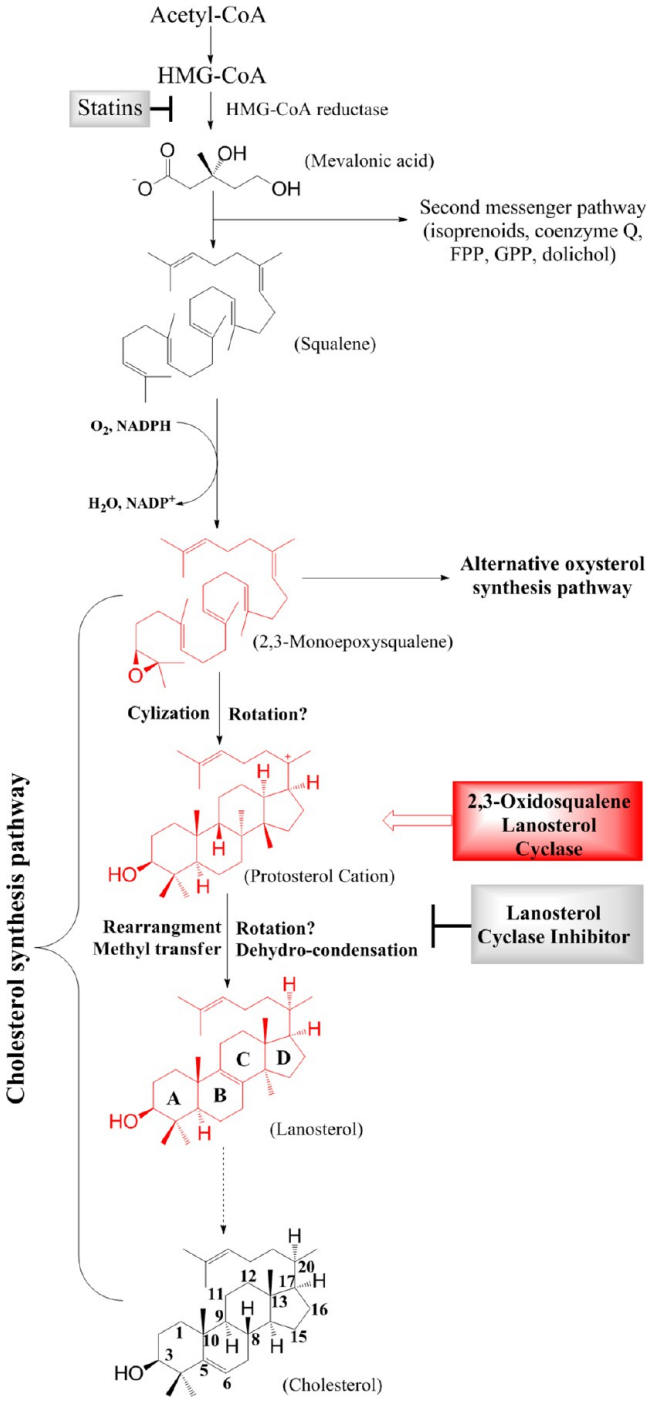

Figure 1. Cholesterol biosynthetic pathway.

protosterol cation), rearrangement, hydrogen transfer, methyl transfer, and dehydro-condensation. Lanosterol is the first sterol to be formed in the MVP and the essential intermediate to form cholesterol.[1,21] This extraordinary reaction has been described as the most complicated enzyme catalytic reaction in human biology.[22] There are two available crystal structures of human OSC (PDB ID: 1W6K and 1W6J):[23] one contains a inhibitor RO48−8071 (1W6J) and the other contains the lanosterol (1W6K). As seen from Figure 2, OSC enzymes are critical to sterol synthesis not only in human being but also in high plants and fungi. There are several OSC isoforms for both sterol synthesis and triterpenoid biosynthesis in the higher plants, such as PNA, bAS, and so on.[24] The biosynthetic diversity of triterpenoids (nearly 200 different cyclic triterpene skeletons) also starts from the cyclization of 2,3-oxidosqualene catalyzed by OSC.[25−27] After constructing the basic cyclic triterpenoid skeletons by OSC, these skeletons can form various cyclic terpene derivatives with oxidation and glycosylation[28,29] Therefore, the cyclization of 2,3-oxidosqualene is the biogenesis origin of the diverse cyclic terpenes. Thus, it is essential to understand the detailed cyclization reaction mechanism of lanosterol biosynthesis that is catalyzed by OSC.

As shown in Figure 1, lanosterol is a tetracyclic triterpenoid with "A−B−C−D" four rings, and the three six-member rings are presented as "chair−boat−chair" conformation (see Figure 2).[30] While the three six-member rings of hopene are presented as "chair−chair−chair" conformation in most cases.[22] Meanwhile, the tailed side chain, which is linked with C_{17} of D-ring (highlighted in red in Figure 3), is β conformation for 2,3-oxidosqualene while it is α conformation in lanosterol. It was reported that the "tail" might rotate from β to α conformation after yielding the protosterol cation.[31] Howevre, the rotation that occurred before or after the protosterol cation was yielded is still unclear due to no direct evidence.[22,32]

The catalytic mechanism of OSC has been debated for more than half a century.[1,24,33−43] Fortunately, the human OSC (LAS) crystal structures was solved several years ago,[23] and several enzyme mutagenesis studies of ERG7 (OSC isoform in *Saccharomyces cerevisiae*) were carried out.[33−38,40,44] So far, some consensuses have been presented, such as, the stepwise path of the whole A−B−C−D ring formation to yield protosterol cation,[42,45,46] the concerted procedure of three-member epoxide-ring-opening and A-ring formation.[42,43,47−49] The cyclization reaction from linear oxidosqualene to the 6−6−5 A−B−C ring is thought to be concerted based on theoretical calculation by Hess and co-workers very recently.[50,51] Nevertheless, many controversies are still unsolved for the cyclization to yield the protosterol cation. As shown in Figure 3, there are three major hypotheses in previous studies,[52−54] and all of these hypotheses have the same initial steps of cyclization but quite different views about the formation of C and D rings. First, it is widely accepted that the epoxide opening and the A-ring formation are concerted and the first intermediate is the A state.[43] Then, the cation transfers from C_{10} to C_8 to yield the B state (B-ring formed). After the B state, hypothesis I proposed that the C-ring can be formed directly through the anti-Markovnikov addition.[23,55] While hypothesis II suggested a stepwise mechanism in which a Markovnikov addition product (C′ state, with a five-membered C-ring) is formed first and followed by a ring expansion to a stable six-membered C-ring (C state).[32,42] Since the 6−6−5 triterpenoid structure motif is common in nature while natural 6−6−6 triterpenoid structure rarely exists, hypothesis II is widely accepted.[27,39,41,56−58] Nevertheless, hypothesis III, proposed by Hess on the basis of ab initio calculations,[42] supported the fact that the 6−6−5 C′ state may directly convert to the 6−6−6−5 D state without the C state intermediate. Furthermore, Eriksson's studies also pointed out the possibility of this concerted reaction.[59] This concerted reaction also existed in another squalene cyclase, squalene-hopene cyclase (SHC).[60] With regard to mutagenesis experiments, it seems that the enzyme reaction would stop at the A state with V454A or V454G mutation in ERG7,[52] whereas the $ERG7^{Y707H}$ mutation can stabilize the bicyclic intermediate B state.[54] Similarly, the $ERG7^{F445T}$ mutation indicated that the C′ state can exist.[53] However, none of the mutation experiments are observed directly in human OSC

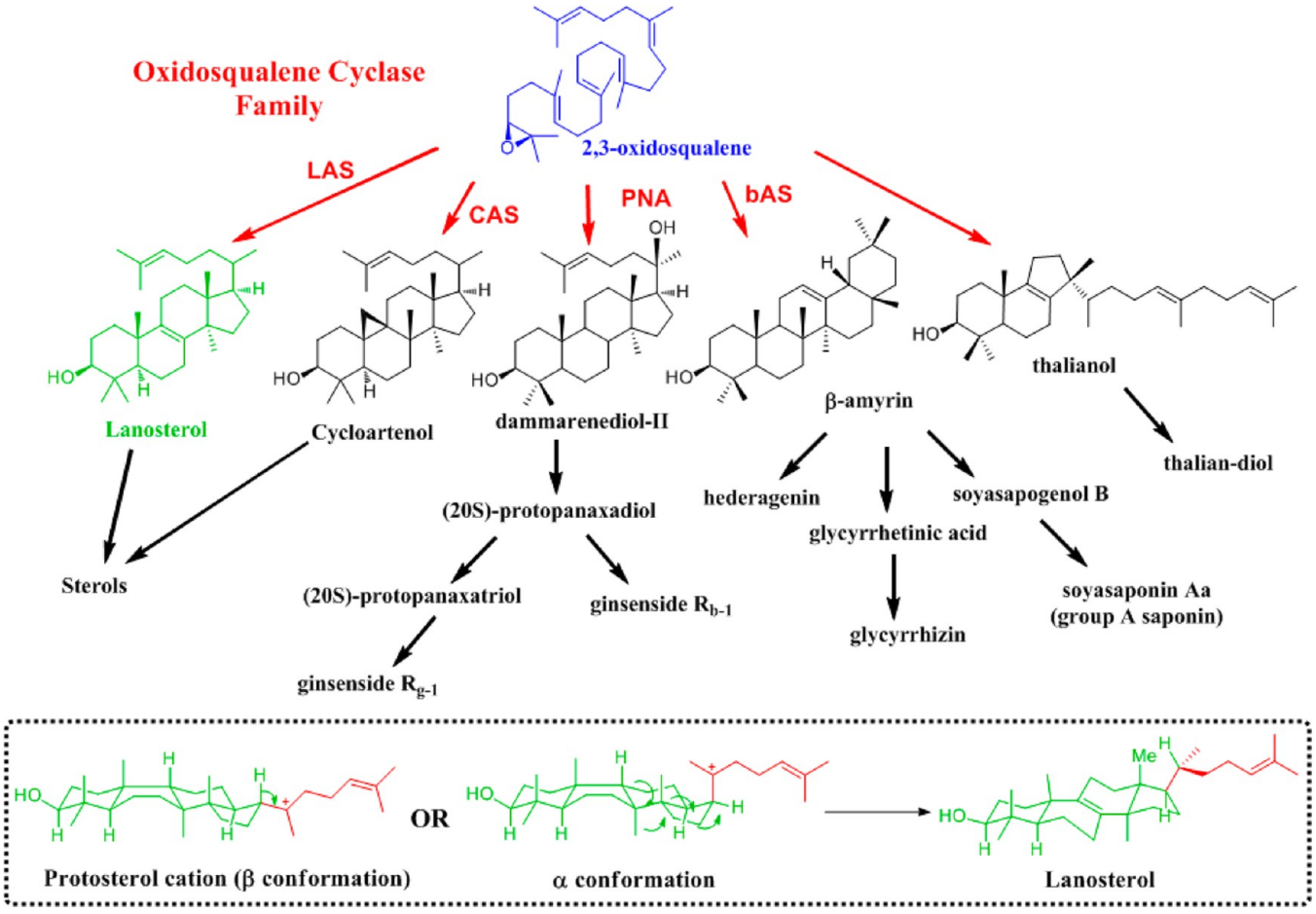

Figure 2. Brief triterpenoid biosynthetic pathway and two possible conformations for the tailed chain of protosterol cation.

(LAS), so it is still uncertain that all of the A, B, C, and C′ states are stable in LAS.

Since there are still so many unclear or controversial problems in lanosterol biosynthesis catalyzed by LAS, herein we focus on the cyclization mechanism studies of C-ring and D-ring via employing combined quantum mechanics and molecular mechanics molecular dynamics (QM/MM MD) simulations, and two controversial issues are addressed: (1) What's the exact cyclization mechanism: by the 6−6−6 or 6−6−5 intermediate? (2) When to transfer β conformation to α conformation for the "tail": before or after the protosterol cation was yielded?

METHODS

I. Preparation of the Enzyme−Ligand Complex. The X-ray crystal structure of LAS was solved in 2004.[23] As shown in Figure 4, the whole structure consists of two (α/α) barrel domains that are connected by loops and three smaller β-sheet structures. The active-site cavity is located between two barrel domains. The LAS is a monotopic membrane protein and just only 6% of the total enzyme surface is membrane-binding region and this region is far away from the active-site.[23] So the protein without membrane was setup for the following simulations. Considering the uncertain conformation of the tailed side chains in the protosterol cation, two models (models A and B, see in Figure 4) were prepared from the crystal structure (PDB ID: 1W6K). The protonation states of charged residues were determined by the PDB2PQR program[61] at pH 8.0 according to the previous experiments.[62] Particularly, the Asp 455 residue, one key residue that was considered as the proton donor to start this cascade reaction, was negative state in this system.

For these models, the AMBER03 force field[63] was employed for the protein and the TIP3P model for water molecules.[64] The force field parameters of ligands were generated from AMBER GAFF force field,[65] and the partial atomic charge of substrates was calculated by the restrained electrostatic potential (RESP)[66] charge from HF/6-31G* calculation with the Gaussian 09 package.[67] Two whole systems were solvated into a ∼102 × 104 × 97 Å rectangular box of TIP3P water molecules. At last, the initial coordinates and topology files were generated by the *tleap* program in AMBER12. Both systems were treated with the same steps during the MD simulations. First, two systems were optimized by multistep minimization. After the optimization, two systems were heated from 0 to 300 K gradually under the NVT ensemble for 100 ps. Then, another 100 ps MD simulations were employed under the NPT ensemble to relax two systems density to be about 1.0 g/cm^3, with the target temperature of 300 K and the target pressure of 1.0 atm. In the NPT ensemble, the Berendsen thermostat method was used to control the system temperature.[68] Finally, a 5 ns MD simulation under the NVT ensemble was carried out via employing the periodic boundary condition. During the MD simulations, the SHAKE algorithm[69] was applied to constrain all hydrogen-containing bonds with a tolerance of 10^{-5}. A cutoff of 12 Å was set for both van der

dx.doi.org/10.1021/ct400949b | J. Chem. Theory Comput. 2014, 10, 1109−1120

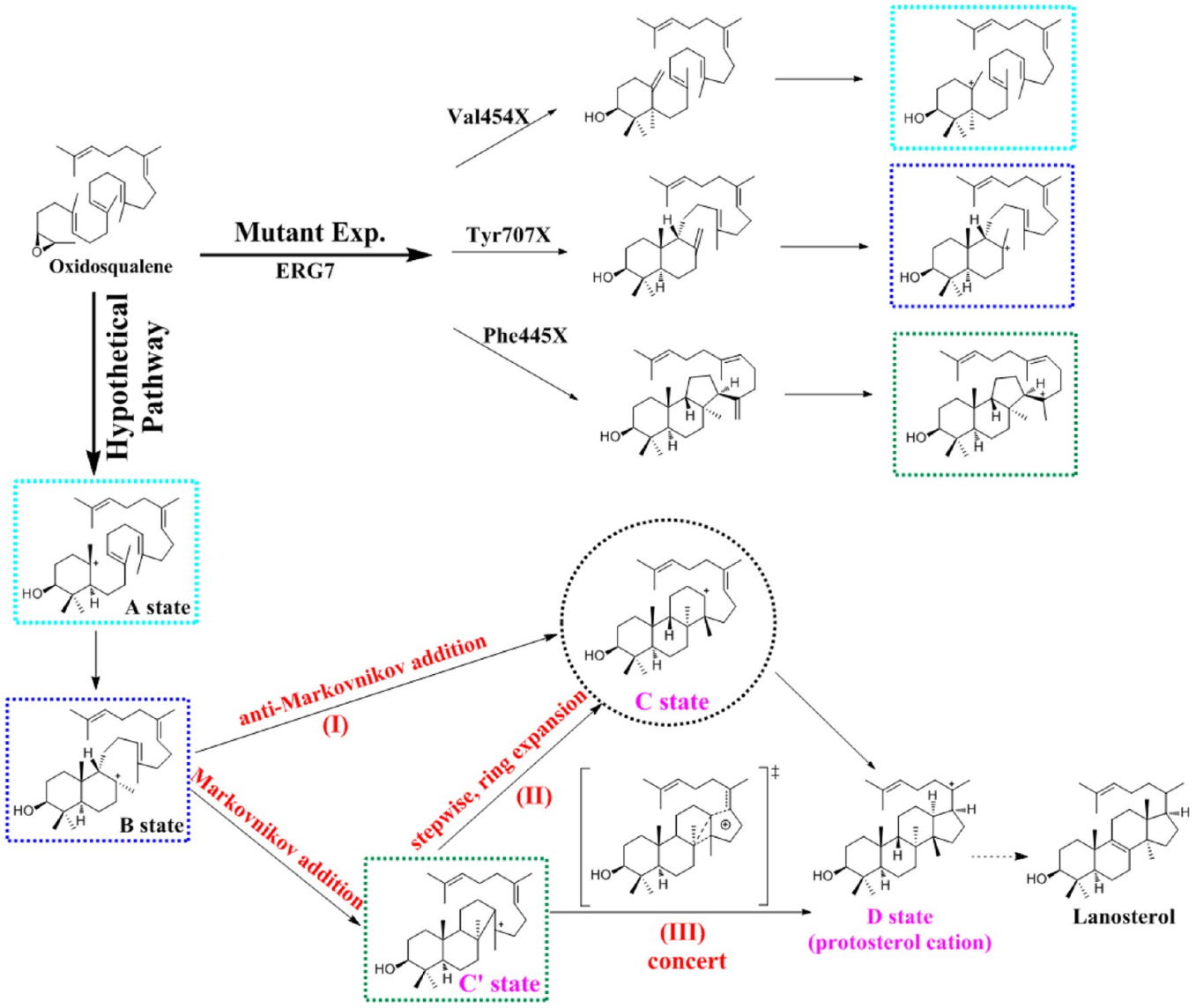

Figure 3. Selected important experimental results for the mutational ERG7 and hypothetic catalytic mechanisms for the human OSC (LAS).

Waals and electrostatic interactions. All simulations were accomplished with the *pmemd* program in AMBER12[70] and the final snapshots of each system from the stable trajectories were used to build the initial structures for the subsequent QM/MM simulations.

II. Setup for QM/MM MD Simulations. Both QM/MM models were prepared by deleting the solvent molecules beyond 36 Å from the C_{16} atom in protosterol cation. After the cutting, the QM/MM area of two models both consist of about 22 000 atoms. As shown in Figure 4, based on the crystal structure, there are two key residues besides the C_{20} and C_{13} cation, so the protosterol cation and both these residues (His 232 and Phe 696) are considered as the QM area. All of these atoms in the QM subsystem were described with the M06-2X[71,72] functional using the 6-31G(d) basis set, and it adds up to 750 basis functions (the benchmark test were performed; see Figure S1−S3 in the Supporting Information). The QM/MM boundary was treated by the improved pseudobond approach.[73−75] In addition, the other atoms were described by the same force field used in classical MD simulations. The spherical boundary condition was employed, and atoms more than 24 Å away from the spherical center were fixed. The 12 and 18 Å cutoffs were employed for van der Waals and electrostatic interactions, respectively.

In order to investigate the cyclization reaction, the sum of d_{C8-C14} and $d_{C13-C17}$ was chosen as the reaction coordinate for both models, and the QM/MM minimization calculation was applied to map out a minimum energy path with the reaction coordinate driving method.[76] After scanning the reaction path of both models, the MM subsystems were further equilibrated by molecular mechanical MD simulation for 500 ps with the frozen QM subsystem. Afterward, the resulting snapshots were treated as the starting structures for ab initio QM/MM MD simulations under the umbrella sampling method. Every window was calculated for 20 ps with 1 fs time step. The system temperature was controlled by the Berendsen thermostat method at 300 K, and the Newton equations of motion were integrate by the Beeman algorithm.[77] After umbrella sampling[78] with biased-potential-based QM/MM MD simulation, the WHAM[79,80] program was applied to calculate the free energy profile with data from each window. All of these ab

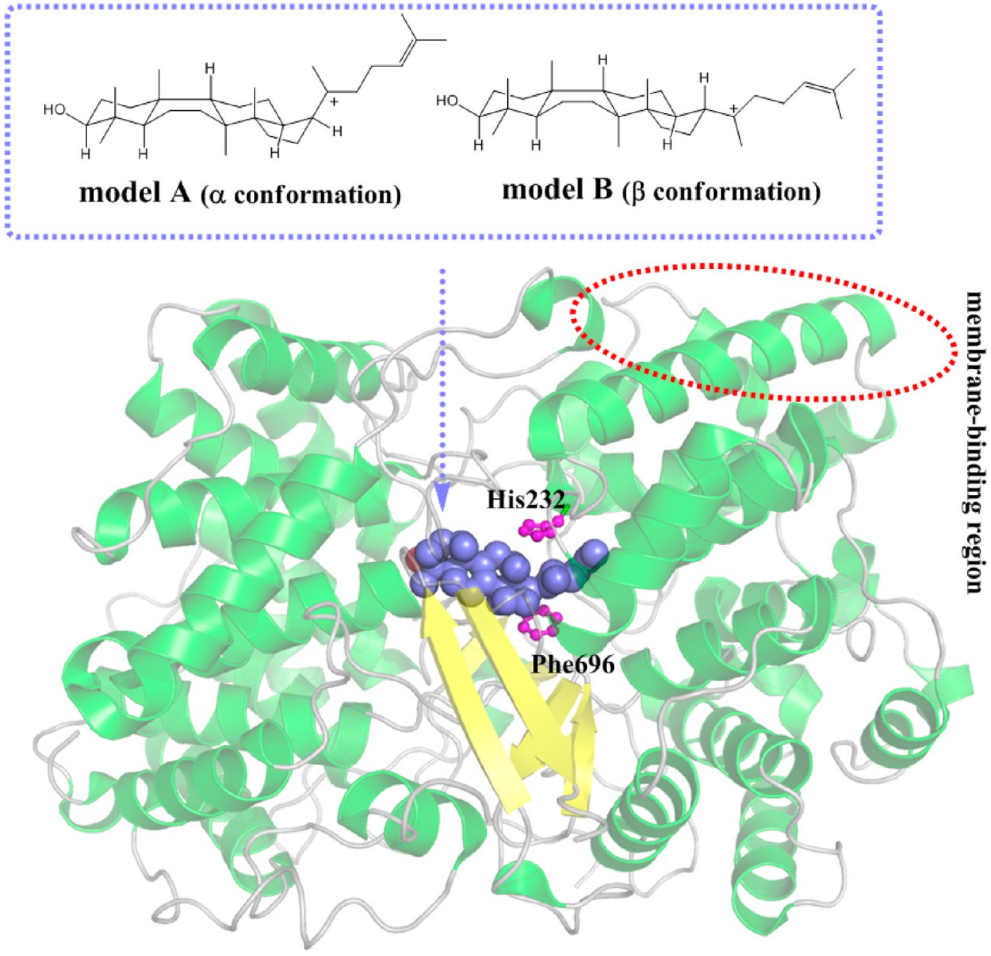

Figure 4. Two computational models built on the LAS crystal structure. QM part consist of the protosterol cation (82 atoms) with/without the His232/Phe696 residues.

initio QM/MM calculations were performed with modified Q-Chem[81] and Tinker[82] programs.

RESULTS AND DISCUSSION

I. Reaction Mechanism. In order to compare the three hypotheses shown in Figure 3, we carried out the QM/MM MD simulations to calculate the reaction energy barrier and verify the local structures in all hypotheses. Since the major difference between the hypotheses I/II and III is whether C state is necessary and exists or not, we tried many protocols to get the C state (as shown in Figure S4 in the Supporting Information): (a) The QM/MM reaction-path-derived scanning with various reaction coordinates, such as the distance of $C_{13}-C_{17}$ (from C state to D state), the one of C_8-C_{14} (from B state to C state), the one from C′ state to C state, and so on; (b) the 8 ns MM MD simulations to maintain the C state artificially, followed by restraint QM/MM optimization and QM/MM MD simulation to obtain the C state, and finally reduce the restraint force to zero step by step. However, all of these attempts failed to get the stable C state. So hypotheses I and II are not supported, while the hypothesis III is the most plausible one based on our simulations. Moreover, hypothesis III is similar to the cyclization step from 6,6,6,5-tetracyclic carbon skeleton to 6,6,6,6,5-pentacyclic hopanoid in the squalene-hopene cyclase.[60]

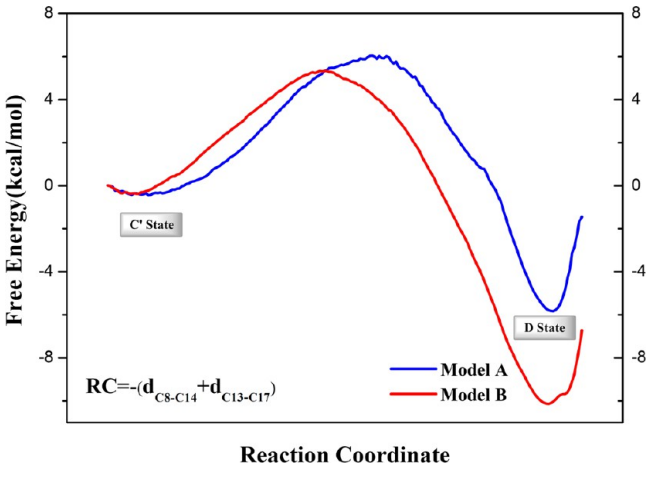

Figure 5. Reaction free energy profiles for the two computational models.

II. Reaction Free Energy Profile. The potential of mean force (PMF) is depicted in Figure 5. It is a concerted reaction without any intermediate from C′ state to D state in both models A and B. And it is thermodynamically and kinetically reasonable due to the exothermicity as well as very low reaction barrier. The barriers are very close (~6.4 and ~5.7 kcal/mol) in both models A and B, and both are a little lower than that of previous ab initio calculations by Hess (8 kcal/mol).[45] It seems that the enzyme environment leads to the lower reaction barrier

dx.doi.org/10.1021/ct400949b | J. Chem. Theory Comput. 2014, 10, 1109−1120

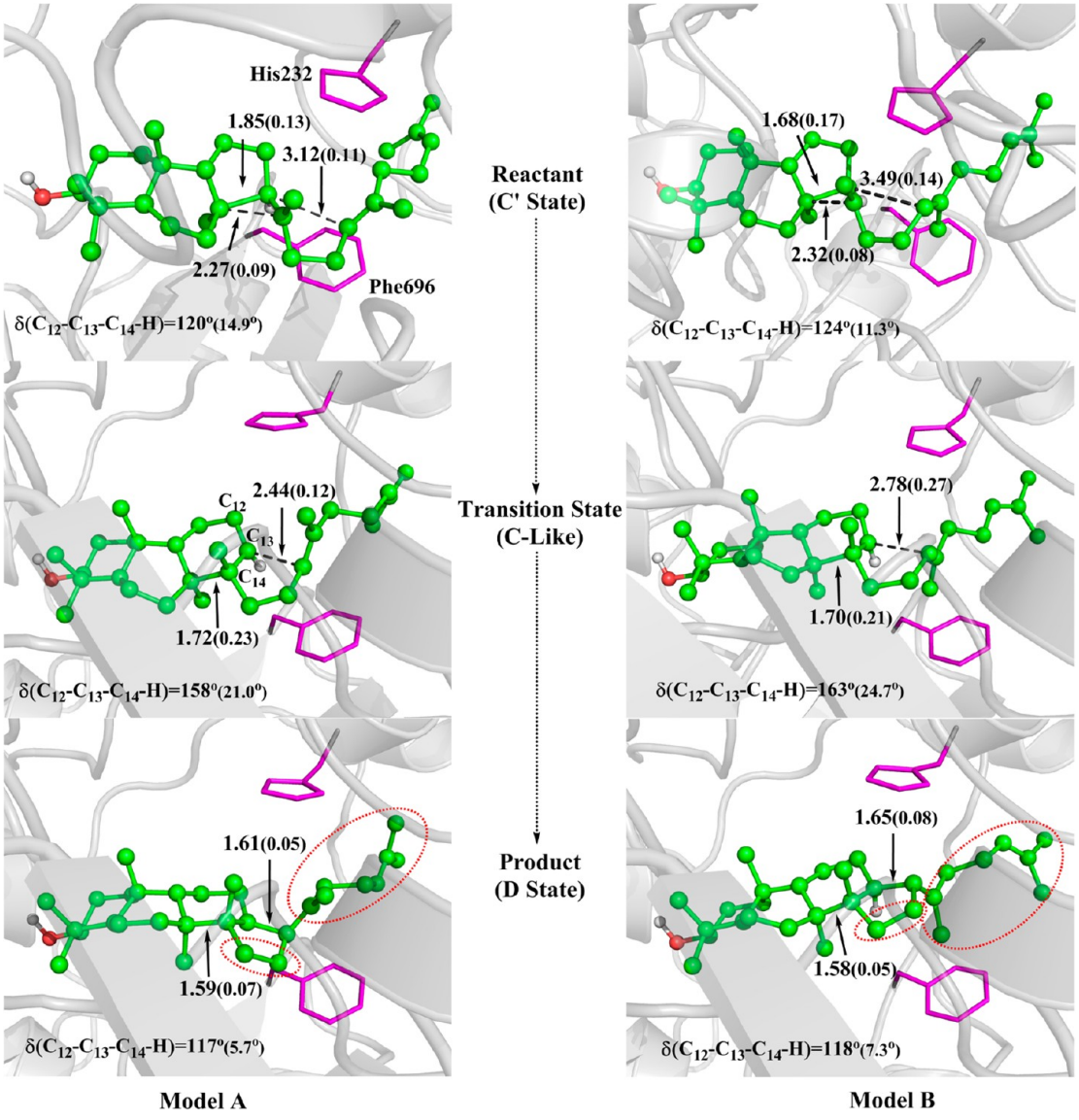

Figure 6. Ligand structures evolution along the cyclization reaction for two models. The numbers in the bracket is the SD values of distances and angles. The selected torsion angles (the H on C_{13}) indicate the hybridization change of C_{13}. The two distinct structure differences at the D state are marked by red dashed circle.

Table 1. Charge Distribution of the Selected Atoms for Each State in the Two Computational Models

	atom name	C′ state	TS	D state
model A	C_{13}	−0.15 ± 0.07	0.34 ± 0.13	0.25 ± 0.09
	C_{14}	0.59 ± 0.12	0.06 ± 0.05	0.10 ± 0.09
	C_{20}	−0.03 ± 0.08	0.20 ± 0.08	0.63 ± 0.17
model B	C_{13}	−0.15 ± 0.09	0.39 ± 0.17	−0.03 ± 0.04
	C_{14}	0.61 ± 0.21	−0.05 ± 0.16	0.21 ± 0.09
	C_{20}	0.14 ± 0.06	0.22 ± 0.08	0.65 ± 0.25

Table 2. Cation−π interaction distance between the carbonium ion and the aromatic ring-center of the two key residues[a]

	C′ state (C_{14}^+)	TS (C_{13}^+)	D state (C_{20}^+)
H232	5.06 ± 0.23, 4.77 ± 0.2	5.18 ± 0.29, 4.81 ± 0.21	4.54 ± 0.21, 4.50 ± 0.20
F696	5.25 ± 0.26, 5.41 ± 0.31	4.78 ± 0.33, 5.68 ± 0.27	4.49 ± 0.23, 4.76 ± 0.18

[a]The first entry is for model A and the second is for model B.

but does not change the concerted reaction mechanism significantly against the gas phase model. Meanwhile, the reaction energy curve progressing from C′ state to transition state is much more smoother while after transition state is more or less steep in both models. Therefore the reaction nature is the same disregarding the "tail" conformation during this cyclization step. However, the stability of the D state is different for the two models (~4 kcal/mol difference). It indicates that the β conformation is much more stable for the protosterol cation (D state). The other difference between the two models is that the TS structure of model B is more or less closer to the C′ state than that of model A. In a word, our calculated reaction free energy profile supports the concerted mechanism (hypothesis III).

III. Structure Motif Evolution along the Reaction. As shown in Figure 6, at the reactant state, the C_8−C_{13} distances are ~1.9 and ~1.7 Å in models A and B, respectively, while the

dx.doi.org/10.1021/ct400949b | J. Chem. Theory Comput. 2014, 10, 1109−1120

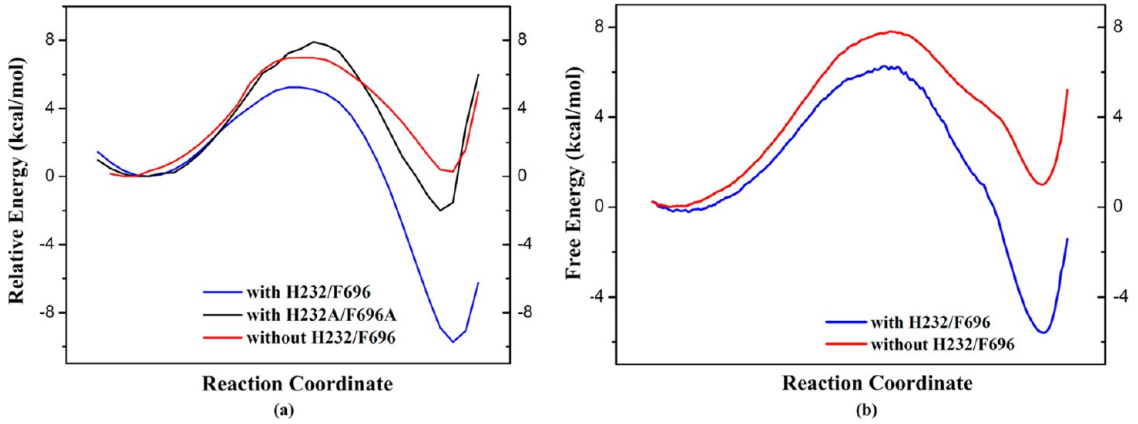

Figure 7. (a) Comparison of the relative energy profiles among three models ("with residues" model: namely model A; "mutation" model: model A with H232A/F696A mutation; "without residues" model: model A with smaller QM size, without H232/F696 in the QM subsystem). (b) Comparison of the free energy profiles between "with residues" and "without residues" models.

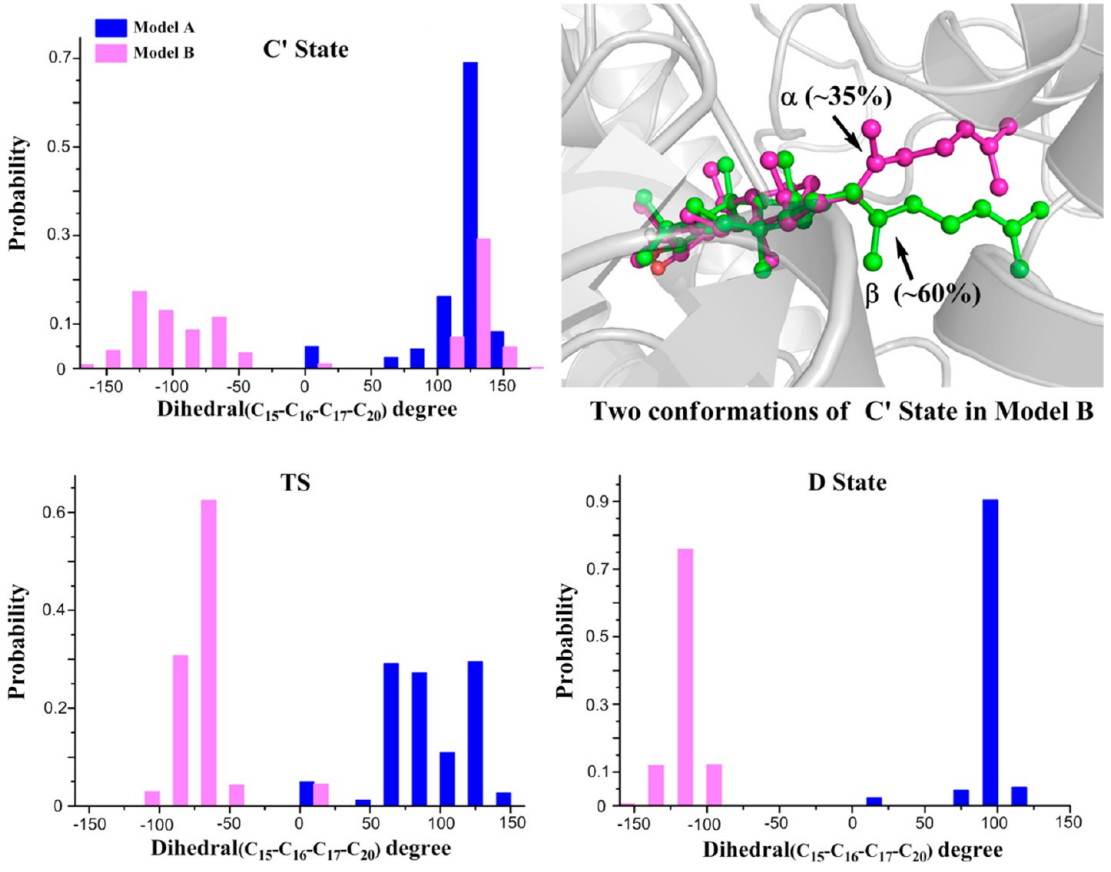

Figure 8. Comparison of conformations and selected dihedral angle distribution at three states along the reaction.

C_8-C_{14} distance is ~2.3 Å in both models. Therefore, the C ring is a five-member ring for two models at the reactant state (viz. the "6−6−5" C′ state described in introduction part). For the transition states, the C_8-C_{14} distances in both models reduce to 1.7 Å, which means that the C ring becomes a six-member ring. Moreover, according to the average dihedral angles for $C_{12}-C_{13}-C_{14}-H$ (Figure 6), it is clear that C_{13} is an sp3 hybridization carbon at the reactant state while it nearly becomes sp2 hybridized at the transition state. Meanwhile, the hybridization type of C_{14} changes from sp2 to sp3 as the reaction proceeds to transition state. Owing to six-member-like C ring and the sp2 hybridization of C_{13}, the "6−6−6" structure motif at transition state is very similar to the "6−6-6" motif of C state as mentioned before. From C′ state to this C-like transition state, d_{C8-C14} decreases by about 0.6 Å as well as $d_{C13-C17}$, while the bond between C_8-C_{13} breaks slowly, making it gently endothermic for this ring-expansion process. On the contrary, d_{C8-C14} and $d_{C13-C17}$ decreasing from C-like transition state to D state to form C−C single bond makes it rapidly exothermic for this ring-close process. It is in agreement with the reaction free energy profile.

IV. Migration and Stability of the Carbon Cation. The ESP charge distribution of the three key atoms (C_{13}, C_{14}, and C_{20}) at each reaction state is shown in Table 1, apparently, from

dx.doi.org/10.1021/ct400949b | J. Chem. Theory Comput. 2014, 10, 1109−1120

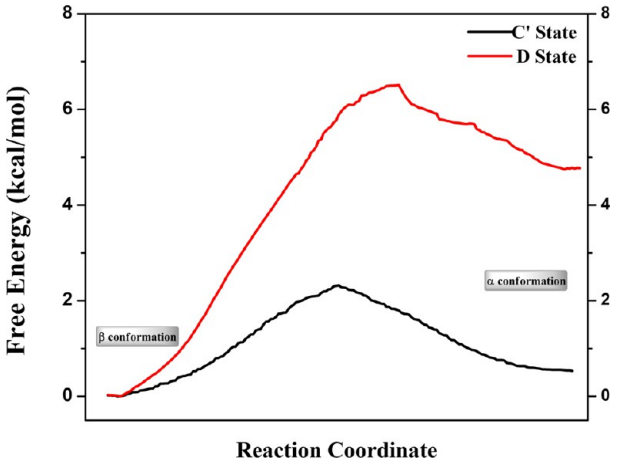

Figure 9. Free energy profiles for the "tail" rotation. The QM/MM FEP calculations are performed 500 ps for each window (every 5 degrees per window).

the reactant state to the product state, followed by positive charge transfer from C_{14} (~0.60) to C_{20} (~0.64) via the C_{13} (~0.36) either in model A or in model B. The essence of this cation migration progress coincides with that of the atom hybridization change (see Figure 6, sp2 hybridization of C_{13} at the C′ state, sp2 hybridization of C_{13} at the C-like TS state, and sp2 hybridization of C_{20} at the D state). Therefore it further clarifies that the nature of this cyclization reaction is electrophilic addition.

According to the positive charge transfer, it is important to stabilize the cation to promote the cyclization reaction. It is reported that cation−π interactions are important and common to disperse high positive charge in polycyclization enzymes.[83,84] In squalene-hopene cyclase, the active site is lined with aromatic residues and the cation−π interactions are ideal for the stabilization of this carbon cation.[85] A similar situation exists in the human OSC system. There are two aromatic residues (His232 and Phe696) around the C and D rings which should be the key residues to make the cation stable. As listed in Table 2, the distances between the carbon cation and centroids of the two aromatic residues are around 4.5 and ~5.2 Å in both models, which present the existence of cation−π interactions.[86]

To identify the contribution of the cation−π interaction, as shown in Figure 7a, we further performed QM/MM scan calculations on the other two computational models to compare with model A. It indicates that the majority of the contribution of the cation−π interaction is to stabilize the D state. Furthermore, the PMF of "with residues" and "without residues" models are plotted in Figure 7b. It indicates that the

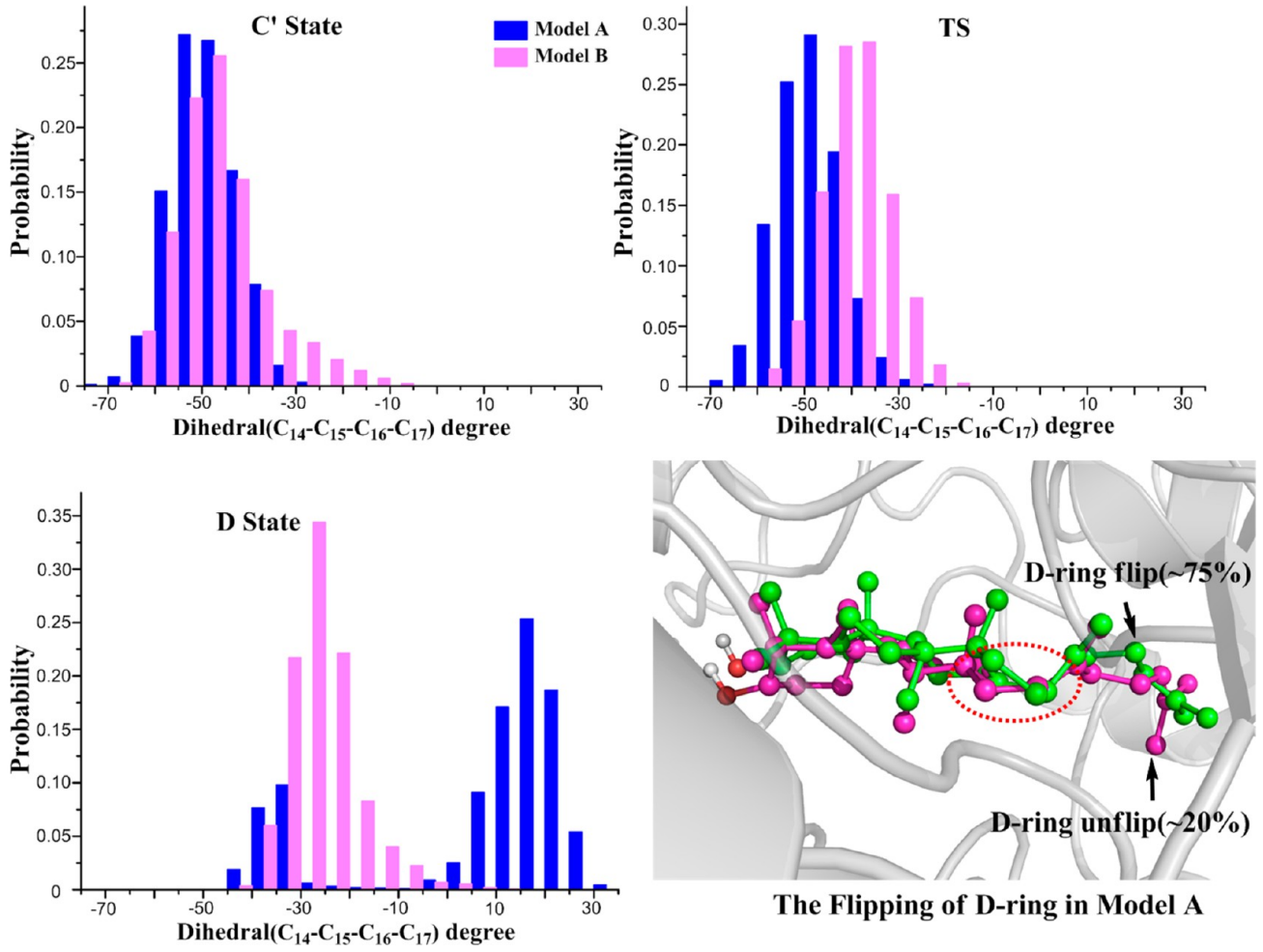

Figure 10. Comparison of the dihedral degree (C_{14}−C_{15}−C_{16}−C_{17}) distribution at three reaction states and the flipping of the D ring skeleton at the D state in model A.

dx.doi.org/10.1021/ct400949b | J. Chem. Theory Comput. 2014, 10, 1109−1120

dispersion effect of positive charge on C_{13} originating from cation−π interactions will stabilize the TS and slightly reduce the reaction barrier (∼ 1.6 kcal/mol). Meanwhile it also obviously stabilizes the D state as the distance between the carbon cation C_{20} and centroids of the aromatic residues is only ∼4.5 Å in model A. Because this very strong cation−π interaction could not be described well at MM level, the D state energy in the "with residues" model is ∼6 kcal/mol lower than that in the "without residues" model. Thus the stabilization of the D state brings the reaction exothermicity.

V. Possible Conformation Change from β to α at C′ State. As shown in Figure 6, the α and β conformation of the tailed side chain can be almost kept either in model A or B along the cyclization. To analyze the conformation change of the "tail", the dihedral degrees distribution has been summarized as histogram plot in Figure 8. Interestingly, it clearly distinguishes the dihedral degree either at the D state or transition state, and the distribution is slightly wider at TS than that at the D state in model B. However, at the C′ state in model B, the dihedral angle distribution is much more dispersed, owing to the fact that there are two main kinds of structures based on structure cluster analysis, nearly 60% β conformation and about 35% α conformation. It is not observed in model A. These conformation analysis results indicate that maybe it is easier to change the conformation from β to α at the C′ state rather than other states. So it is further proposed that the rotation of the "tail" will be restrained because the D ring is already cyclized at the D state (6−6−6−5 tetracycles) while it is not yet at the C′ state (6−6−5 tricycles) and C-like transition state (6−6−6 tricycles).

In order to further demonstrate the "tail" rotation characteristic along the reaction, the rotation energy profile from β to α conformations at the C′ and D states has been obtained by QM/MM free energy perturbation (FEP) calculations. As shown in Figure 9, the energy barrier of the rotation at C′ state is only about 2 kcal/mol, so that it can occur conformation transfer spontaneously. But the barrier at D state is about 3 times higher than that at C′ state. Therefore, our calculations support that the "tail" rotation is preferred to take place before the formation of protosterol cation (D state) instead of after protosterol cation formed.

VI. Skeleton Hopping of the D Ring. As seen in Figure 6, the D ring skeleton overturns after the cyclization in model A while there is no flipping observed in model B. As shown in Figure 10, it presents a similar distribution for the selected dihedral angle either at the C′ or transition state. However, it showsa totally different distribution at the D state due to the ring-skeleton hopping occurring in model A. According to the structure cluster analysis, nearly 75% is flipped while just only about 20% is not. On the basis of the previous assumptions, the D ring would twist after the formation of α conformation protosterol cation.[23,31] Nevertheless, in our simulations, the D ring twists during the cyclization once α conformation is formed, while the skeleton hopping does not occur in the case of the β conformation. Therefore, it is possible that the "tail" rotation from β to α will happen at (or before) the C′ state and followed by the D ring hopping once the cyclization is finished by human OSC catalysis.

CONCLUSION

The ab initio QM/MM MD simulations indicate that the cyclization from the C′ state (6−6−5) to the D state (6−6−6−5) catalyzed by OSC is a concerted process. The C′ and D states are both the stable intermediates during the catalytic reaction. As for the C state (6−6−6), which was considered to be a stable intermediate before, it is very similar to the transition state in our simulations. Furthermore, we propose that the "tail" rotation (viz. conformation change from β to α) can happen at the C′ state due to the very low energy barrier. The flipping of the D ring can occur in the case of the α conformation protosterol cation yielded. Both the tail rotation and ring hopping will make the conformation of the protosterol cation more similar to that of lanosterol.

ASSOCIATED CONTENT

Supporting Information

Benchmark test on the different methods and basis sets as well as all protocols used to obtain C state. This material is available free of charge via the Internet at http://pubs.acs.org.

AUTHOR INFORMATION

Corresponding Authors

*E-mail: xujun9@mail.sysu.edu.cn.
*E-mail: wurb3@mail.sysu.edu.cn.

Notes

The authors declare no competing financial interest.

ACKNOWLEDGMENTS

This work was supported by the National Science Foundation of China (21203257 and 21272289). We thank the National Supercomputing Center in Shenzhen, Guangzhou and Tianjin, and the Guangdong Province Key Laboratory of Computational Science and the Guangdong Province Computational Science Innovative Research Team for providing the computational resources. We also thank Dr. Shenglong Wang at NYU-ITS for his kind help.

REFERENCES

(1) Bloch, K. The biological synthesis of cholesterol. *Science* **1965**, *150* (3692), 19−28.
(2) Goldstein, J. L.; Brown, M. S. Regulation of the mevalonate pathway. *Nature* **1990**, *343* (6257), 425−430.
(3) Marinier, E.; Lincoln, B. C.; Garneau, M.; David, F.; Brunengraber, H. Contribution of the shunt pathway of mevalonate metabolism to the regulation of cholesterol synthesis in rat liver. *J. Biol. Chem.* **1987**, *262* (35), 16936−16940.
(4) Ohvo-Rekila, H.; Ramstedt, B.; Leppimaki, P.; Slotte, J. P. Cholesterol interactions with phospholipids in membranes. *Prog. Lipid Res.* **2002**, *41* (1), 66−97.
(5) Yeagle, P. L. Modulation of membrane function by cholesterol. *Biochimie* **1991**, *73* (10), 1303−1310.
(6) Haines, T. H. Do sterols reduce proton and sodium leaks through lipid bilayers? *Prog. Lipid Res.* **2001**, *40* (4), 299−324.
(7) Incardona, J. P.; Eaton, S. Cholesterol in signal transduction. *Curr. Opin. Cell Biol.* **2000**, *12* (2), 193−203.
(8) Smith, L. L. Another cholesterol hypothesis: Cholesterol as antioxidant. *Free Radic. Biol. Med.* **1991**, *11* (1), 47−61.
(9) Durrington, P. Dyslipidaemia. *Lancet* **2003**, *362* (9385), 717−731.
(10) Carmena, R.; Duriez, P.; Fruchart, J. C. Atherogenic lipoprotein particles in atherosclerosis. *Circulation* **2004**, *109* (23 Suppl 1), III2−7.
(11) Istvan, E. S.; Deisenhofer, J. Structural mechanism for statin inhibition of HMG-CoA reductase. *Science* **2001**, *292* (5519), 1160−1164.
(12) Grundy, S. M.; Cleeman, J. I.; Merz, C. N.; Brewer, H. B., Jr.; Clark, L. T.; Hunninghake, D. B.; Pasternak, R. C.; Smith, S. C., Jr.; Stone, N. J. Coordinating Committee of the National Cholesterol Education, P. Implications of recent clinical trials for the National

Cholesterol Education Program Adult Treatment Panel III Guidelines. *J. Am. Coll. Cardiol.* **2004**, *44* (3), 720−732.
(13) Craine New York Business http://www.crainsnewyork.com/article/20111228/HEALTH_CARE/111229902#; published 12/28/2011; accessed 10/30/2013.
(14) Brown, M. S.; Goldstein, J. L. Multivalent feedback regulation of HMG CoA reductase, a control mechanism coordinating isoprenoid synthesis and cell growth. *J. Lipid. Res.* **1980**, *21*, 505−517.
(15) Pedersen, T. R.; Tobert, J. A. Benefits and risks of HMG-CoA reductase inhibitors in the prevention of coronary heart disease: a reappraisal. *Drug Saf.* **1996**, *14* (1), 11−24.
(16) Bellosta, S.; Paoletti, R.; Corsini, A. Safety of statins: focus on clinical pharmacokinetics and drug interactions. *Circulation* **2004**, *109* (23 Suppl 1), III50−57.
(17) Aminopropylindenes derived from Grundmann's ketone as a novel chemotype of oxidosqualene cyclase inhibitors. Staedler, D.; Chapuis-Bernasconi, C.; Dehmlow, H.; Fischer, H.; Juillerat-Jeanneret, L.; Aebi, J. D. Cytotoxic effects of combination of oxidosqualene cyclase inhibitors with atorvastatin in human cancer cells. *J. Med. Chem.* **2012**, *55* (11), 4990−5002.
(18) Lange, S.; Keller, M.; Muller, C.; Oliaro-Bosso, S.; Balliano, G.; Bracher, F. Aminopropylindenes derived from Grundmann's ketone as a novel chemotype of oxidosqualene cyclase inhibitors. *Eur. J. Med. Chem.* **2013**, *63*, 758−764.
(19) Lenhart, A.; Reinert, D. J.; Aebi, J. D.; Dehmlow, H.; Morand, O. H.; Schulz, G. E. Binding structures and potencies of oxidosqualene cyclase inhibitors with the homologous squalene-hopene cyclase. *J. Med. Chem.* **2003**, *46* (11), 2083−2092.
(20) Abe, I.; Zheng, Y. F.; Prestwich, G. D. Photoaffinity labeling of oxidosqualene cyclase and squalene cyclase by a benzophenone-containing inhibitor. *Biochemistry* **1998**, *37* (17), 5779−5784.
(21) Huff, M. W.; Telford, D. E. Lord of the rings–the mechanism for oxidosqualene:lanosterol cyclase becomes crystal clear. *Trends Pharmacol. Sci.* **2005**, *26* (7), 335−340.
(22) Wendt, K. U.; Schulz, G. E.; Corey, E. J.; Liu, D. R. Enzyme Mechanisms for Polycyclic Triterpene Formation. *Angew. Chem., Int. Ed. Engl.* **2000**, *39* (16), 2812−2833.
(23) Thoma, R.; Schulz-Gasch, T.; D'Arcy, B.; Benz, J.; Aebi, J.; Dehmlow, H.; Hennig, M.; Stihle, M.; Ruf, A. Insight into steroid scaffold formation from the structure of human oxidosqualene cyclase. *Nature* **2004**, *432* (7013), 118−122.
(24) Abe, I.; Rohmer, M.; Prestwich, G. D. Enzymatic cyclization of squalene and oxidosqualene to sterols and triterpenes. *Chem. Rev.* **1993**, *93*, 2189−2206.
(25) Ohyama, K.; Suzuki, M.; Kikuchi, J.; Saito, K.; Muranaka, T. Dual biosynthetic pathways to phytosterol via cycloartenol and lanosterol in Arabidopsis. *Proc. Natl. Acad. Sci. U.S.A.* **2009**, *106* (3), 725−730.
(26) Connolly, J. D.; Hill, R. A. Triterpenoids. *Nat. Prod. Rep.* **2002**, *19* (4), 494−513.
(27) Xu, R.; Fazio, G. C.; Matsuda, S. P. On the origins of triterpenoid skeletal diversity. *Phytochemistry* **2004**, *65* (3), 261−291.
(28) Kahn, R. A.; Durst, F. Function and evolution of plant cytochrome P450. *Recent Adv. Phytochem.* **2000**, *34*, 151−189.
(29) Paquette, S.; Moller, B. L.; Bak, S. On the origin of family 1 plant glycosyltransferases. *Phytochemistry* **2003**, *62* (3), 399−413.
(30) Nes, W. D. Biosynthesis of cholesterol and other sterols. *Chem. Rev.* **2011**, *111* (10), 6423−6451.
(31) Wu, T. K.; Chang, C. H.; Liu, Y. T.; Wang, T. T. Saccharomyces cerevisiae oxidosqualene-lanosterol cyclase: a chemistry-biology interdisciplinary study of the protein's structure-function-reaction mechanism relationships. *Chem. Rec.* **2008**, *8* (5), 302−325.
(32) Wu, T. K.; Chang, C. H.; Liu, Y. T.; Wang, T. T. Saccharomyces cerevisiae Oxidosqualene-Lanosterol Cyclase: A Chemistry-Biology Interdisciplinary Study of the Protein's Structure-Function-Reaction Mechanism Relationships. *Chem. Rec.* **2008**, *8* (5), 302−325.
(33) Woodward, R. B.; Bloch, K. The cyclization of squalene in cholesterol synthesis. *J. Am. Chem. Soc.* **1953**, *75*, 2023−2024.
(34) Eschenmoser, A.; Ruzicka, L.; Jeger, O.; Arigoni, D. Zur kenntnis der triterpene: Eine stereochemische interpretation der biogenetischen isoprenregel bei den triterpenen. *Helv. Chim. Acta* **1955**, *38*, 1890−1904.
(35) Stork, G.; Burgstahler, A. W. The stereochemistry of polymere cyclization. *J. Am. Chem. Soc.* **1955**, *77*, 5068−5077.
(36) Corey, E. J.; Russey, W. E. Metabolic fate of 10,11-dihydrosqualene in sterol-producing rat liver homogenate. *J. Am. Chem. Soc.* **1966**, *88* (20), 4751−4752.
(37) Van Tamelen, E. E.; Willet, J.; Schwartz, M.; Nadeau, R. Nonenzymic laboratory cyclization of squalene 2,3-oxide. *J. Am. Chem. Soc.* **1966**, *88* (24), 5937−5938.
(38) Van Tamelen, E. E.; Willett, J. D.; Clayton, R. B.; Lord, K. E. Enzymic conversion of squalene 2,3-oxide to lanosterol and cholesterol. *J. Am. Chem. Soc.* **1966**, *88* (20), 4752−4754.
(39) Van Tamelen, E. E.; Sharpless, K. B.; Hanzlik, R. P.; Clayton, R. B.; Burlingame, A. L.; Wszolek, P. C. Enzymic cyclization of trans,trans,trans-18,19-dehydrosqualene 2,3-oxide. *J. Am. Chem. Soc.* **1967**, *89*, 7150−7151.
(40) Willett, J. D.; Sharpless, K. B.; Lord, K. E.; van Tamelen, E. E.; Clayton, R. B. Squalene-2,3oxide, an intermediate in the enzymatic conversion of squalene to lanosterol and cholesterol. *J. Biol. Chem.* **1967**, *242* (18), 4182−4191.
(41) Corey, E. J.; Cheng, H. Conversion of a C20 2,3-Oxidosqualene Analog to Tricyclic Structures with a Five-Membered C-Ring by Lanosterol Synthase. Further Evidence For a C-Ring Expansion Step in Sterol Biosynthesis. *Tetrahedron Lett.* **1996**, *37*, 2709−2712.
(42) Corey, E. J.; Cheng, H.; Baker, C. H.; Matsuda, S. P. T.; Li, D.; Song, X. Methodology for the Preparation of Pure Recombinant S. cerevisiae Lanosterol Synthase Using a Baculovirus Expression System. Evidence That Oxirane Cleavage and A-Ring Formation Are Concerted in the Biosynthesis of Lanosterol from 2,3-Oxidosqualene. *J. Am. Chem. Soc.* **1997**, *120*, 1277−1288.
(43) Gao, D.; Pan, Y.-K.; Byun, K.; Gao, J. Theoretical Evidence for a Concerted Mechanism of the Oxirane Cleavage and A-Ring Formation in Oxidosqualene Cyclization. *J. Am. Chem. Soc.* **1998**, *120*, 4045−4046.
(44) Barton, D. H. R.; Jarman, T. R.; Watson, K. C.; Widdowson, D. A.; Boar, R. B.; Damps, K. Investiga-tions on the biosynthesis of steroids and terpenoids. Part XII. Biosynthesis of 3β-hydroxy-triterpenoids and-steroids from (3S)-2,3-epoxy-2,3-dihydrosqualene. *J. Chem. Soc., Perkin Trans. 1* **1975**, 1134−1138.
(45) Hess, B. A., Jr. Concomitant C-ring Expansion and D-ring formation in lanosterol biosynthesis from squalene without violation of Markovnikov's rule. *J. Am. Chem. Soc.* **2002**, *124* (35), 10286−10287.
(46) Tantillo, D. J. Biosynthesis via carbocations: theoretical studies on terpene formation. *Nat. Prod. Rep.* **2011**, *28* (6), 1035−1053.
(47) Williams, A. *Concerted Organic and Bio-Organic Mechanisms*; CRC Press: Boca Raton, FL, 2000.
(48) Tantillo, D. J. Recent excursions to the borderlands between the realms of concerted and stepwise: carbocation cascades in natural products biosynthesis. *J. Phys. Org. Chem.* **2008**, *21* (7−8), 561−570.
(49) Michael, J. S. D. Multibond Reactions Cannot Normally Be Synchronous. *J. Am. Chem. Soc.* **1984**, *106*, 209−219.
(50) Hess, B. A., Jr. Formation of the C ring in the lanosterol biosynthesis from squalene. *Org. Lett.* **2003**, *5* (2), 165−167.
(51) Hess, B. A., Jr.; Smentek, L. The concerted nature of the cyclization of squalene oxide to the protosterol cation. *Angew. Chem., Int. Ed. Engl.* **2013**, *52* (42), 11029−11033.
(52) Joubert, B. M.; Ling, H.; Matsuda, S. P. T. Steric Bulk at Position 454 in Saccharomyces cerevisiae Lanosterol Synthase Influences B-Ring Formation but Not Deprotonation. *Org. Lett.* **2000**, *2*, 339−341.
(53) Wu, T. K.; Liu, Y. T.; Chiu, F. H.; Chang, C. H. Phenylalanine 445 within oxidosqualene-lanosterol cyclase from Saccharomyces cerevisiae influences C-ring cyclization and deprotonation reactions. *Org. Lett.* **2006**, *8* (21), 4691−4694.
(54) Wu, T. K.; Wang, T. T.; Chang, C. H.; Liu, Y. T.; Shie, W. S. Importance of Saccharomyces cerevisiae Oxidosqualene-Lanosterol

Cyclase Tyrosine 707 Residue for Chair-Boat Bicyclic Ring Formation and Deprotonation Reactions. *Org. Lett.* **2008**, *10* (21), 4959−4962.
(55) Hoshino, T.; Sato, T. Squalene-hopene cyclase: catalytic mechanism and substrate recognition. *Chem. Commun.* **2002**, No. 4, 291−301.
(56) Hoshino, T.; Sakai, Y. Further evidence that the polycyclization reaction by oxidosqualene-lanosterol cyclase proceeds via a ring expansion of the 5-membered C-ring formed by Markovnikov closure. On the enzymic products of the oxidosqualene analogue having an ethyl residue at the 15-position. *Chem. Commun.* **1998**, *15*, 1591−1592.
(57) Hoshino, T.; Kouda, M.; Abe, T.; Ohashi, S. New cyclization mechanism for squalene: a ring-expansion step for the five-membered C-ring intermediate in hopene biosynthesis. *Biosci. Biotechnol. Biochem.* **1999**, *63* (11), 2038−2041.
(58) Matsuda, S. P. T.; Wilson, W. K.; Xiong, Q. B. Mechanistic insights into triterpene synthesis from quantum mechanical calculations. Detection of systematic errors in B3LYP cyclization energies. *Org. Biomol. Chem.* **2006**, *4* (3), 530−543.
(59) Tian, B. X.; Eriksson, L. A. Catalytic mechanism and product specificity of oxidosqualene-lanosterol cyclase: a QM/MM study. *J. Phys. Chem. B* **2012**, *116* (47), 13857−13862.
(60) Rajamani, R.; Gao, J. Balancing kinetic and thermodynamic control: the mechanism of carbocation cyclization by squalene cyclase. *J. Am. Chem. Soc.* **2003**, *125* (42), 12768−12781.
(61) Dolinsky, T. J.; Nielsen, J. E.; McCammon, J. A.; Baker, N. A. PDB2PQR: an automated pipeline for the setup, execution, and analysis of Poisson-Boltzmann electrostatics calculations. *Nucleic Acids Res.* **2004**, *32*, W665−W667.
(62) Ke, Z.; Guo, H.; Xie, D.; Wang, S.; Zhang, Y. Ab initio QM/MM free-energy studies of arginine deiminase catalysis: the protonation state of the Cys nucleophile. *J. Phys. Chem. B* **2011**, *115* (13), 3725−3733.
(63) Duan, Y.; Wu, C.; Chowdhury, S.; Lee, M. C.; Xiong, G.; Zhang, W.; Yang, R.; Cieplak, P.; Luo, R.; Lee, T.; Caldwell, J.; Wang, J.; Kollman, P. A point-charge force field for molecular mechanics simulations of proteins based on condensed-phase quantum mechanical calculations. *J. Comput. Chem.* **2003**, *24* (16), 1999−2012.
(64) Jorgensen, W. L.; Chandrasekhar, J.; Madura, J. D.; Impey, R. W.; Klein, M. L. Comparison of simple potential functions for simulating liquid water. *J. Chem. Phys.* **1983**, *79*, 926.
(65) Wang, J.; Wolf, R. M.; Caldwell, J. W.; Kollman, P. A.; Case, D. A. Development and testing of a general amber force field. *J. Comput. Chem.* **2004**, *25* (9), 1157−1174.
(66) Bayly, C. I. C. P.; Cornell, W.; Kollman, P. A. A well-behaved electrostatic potential based method using charge restraints for deriving atomic charges: the RESP model. *J. Phys. Chem.* **1993**, *97*, 10269−10280.
(67) Frisch, M. J.; Trucks, G. W.; Schlegel, H. B.; Scuseria, G. E.; Robb, M. A.; Cheeseman, J. R.; Scalmani, G.; Barone, V.; Mennucci, B.; Petersson, G. A.; Nakatsuji, H.; Caricato, M.; Li, X.; Hratchian, H. P.; Izmaylov, A. F.; Bloino, J.; Zheng, G.; Sonnenberg, J. L.; Hada, M.; Ehara, M.; Toyota, K.; Fukuda, R.; Hasegawa, J.; Ishida, M.; Nakajima, T.; Honda, Y.; Kitao, O.; Nakai, H.; Vreven, T.; Montgomery, J. A., Jr.; Peralta, J. E.; Ogliaro, F.; Bearpark, M.; Heyd, J. J.; Brothers, E.; Kudin, K. N.; Staroverov, V. N.; Kobayashi, R.; Normand, J.; Raghavachari, K.; Rendell, A.; Burant, J. C.; Iyengar, S. S.; Tomasi, J.; Cossi, M.; Rega, N.; Millam, J. M.; Klene, M.; Knox, J. E.; Cross, J. B.; Bakken, V.; Adamo, C.; Jaramillo, J.; Gomperts, R.; Stratmann, R. E.; Yazyev, O.; Austin, A. J.; Cammi, R.; Pomelli, C.; Ochterski, J. W.; Martin, R. L.; Morokuma, K.; Zakrzewski, V. G.; Voth, G. A.; Salvador, P.; Dannenberg, J. J.; Dapprich, S.; Daniels, A. D.; Farkas, Ö.; Foresman, J. B.; Ortiz, J. V.; Cioslowski, J.; Fox, D. J. *Gaussian 09*, revision A.1; Gaussian Inc.: Wallingford, CT, 2009.
(68) Berendsen, H. J. C.; Postma, J. P. M.; Van Gunsteren, W. F.; DiNola, A.; Haak, J. R. Molecular dynamics with coupling to an external bath. *J. Chem. Phys.* **1984**, *81*, 3684−3690.
(69) Ryckaert, J. P. C. G.; Berendsen, H. J. C. Numerical integration of the cartesian equations of motion of a system with constraints: molecular dynamics of n-alkanes. *J. Comput. Phys.* **1977**, *23*, 327−341.
(70) Case, D. A.; Darden, T. A.; Cheatham, T. E., III; Simmerling, C. L.; Wang, J.; Duke, R. E.; Luo, R.; Walker, R. C.; Zhang, W.; Merz, K. M.; Roberts, B.; Hayik, S.; Roitberg, A.; Seabra, G.; Swails, J.; Goetz, A. W.; Kolossváry, I.; Wong, K. F.; Paesani, F.; Vanicek, J.; Wolf, R. M.; Liu, J.; Wu, X.; Brozell, S. R.; Steinbrecher, T.; Gohlke, H.; Cai, Q.; Ye, X.; Wang, J.; Hsieh, M. J.; Cui, G.; Roe, D. R.; Mathews, D. H.; Seetin, M. G.; Salomon-Ferrer, R.; Sagui, C.; Babin, V.; Luchko, T.; Gusarov, S.; Kovalenko, A.; Kollman, P. A. *AMBER12*; University of California: San Francisco, CA, 2012.
(71) Zhao, Y.; Truhlar, D. G. The M06 suite of density functionals for main group thermochemistry, thermochemical kinetics, noncovalent interactions, excited states, and transition elements: two new functionals and systematic testing of four M06-class functionals and 12 other functionals. *Theor. Chem. Acc.* **2008**, *120* (1−3), 215−241.
(72) Zhao, Y.; Truhlar, D. G. Exploring the Limit of Accuracy of the Global Hybrid Meta Density Functional for Main-Group Thermochemistry, Kinetics, and Noncovalent Interactions. *J. Chem. Theory Comput.* **2008**, *4* (11), 1849−1868.
(73) Zhang, Y.; Lee, T. S.; Yang, W. A Pseudobond Approach to Combining Quantum Mechanical and Molecular Mechanical Methods. *J. Chem. Phys.* **1999**, *110*, 46−54.
(74) Chen, X.; Zhang, Y.; Zhang, J. Z. An efficient approach for ab initio energy calculation of biopolymers. *J. Chem. Phys.* **2005**, *122* (18), 184105.
(75) Zhang, Y. Pseudobond ab initio QM/MM approach and its Applications to Enzyme Reactions. *Theor. Chem. Acc.* **2006**, *116* (43−50), Special Issue of 'New Perspectives in Theoretical Chemistry'.
(76) Zhang, Y.; Liu, H.; Yang, W. Free energy calculations on enzyme reactions with an efficient iterative procedure to determine minimum energy paths on a combined ab initio QM/MM potential. *J. Chem. Phys.* **2000**, *112*, 3483−3492.
(77) Beeman, D. Some multistep methods for use in molecular dynamics calculations. *J. Comput. Phys.* **1976**, *20*, 131−139.
(78) Torrie, G. M.; Valleau, J. P. Nonphysical sampling distributions in Monte Carlo free-energy estimation: Umbrella sampling. *J. Comput. Phys.* **1977**, *23* (2), 187−199.
(79) Souaille, M.; Roux, B. Extension to the weighted histogram analysis method: combining umbrella sampling with free energy calculations. *Comput. Phys. Commun.* **2001**, *135*, 40−57.
(80) Kumar, S.; Bouzida, D.; Swendsen, R. H.; Kollman, P. A.; Rosenberg, J. M. The weighted histogram analysis method for free-energy calculations on biomolecules. *J. Comput. Chem.* **1992**, *13*, 1011−1021.
(81) Shao, Y.; Molnar, L. F.; Jung, Y.; Kussmann, J.; Ochsenfeld, C.; Brown, S. T.; Gilbert, A. T.; Slipchenko, L. V.; Levchenko, S. V.; O'Neill, D. P.; DiStasio, R. A., Jr.; Lochan, R. C.; Wang, T.; Beran, G. J.; Besley, N. A.; Herbert, J. M.; Lin, C. Y.; Van Voorhis, T.; Chien, S. H.; Sodt, A.; Steele, R. P.; Rassolov, V. A.; Maslen, P. E.; Korambath, P. P.; Adamson, R. D.; Austin, B.; Baker, J.; Byrd, E. F.; Dachsel, H.; Doerksen, R. J.; Dreuw, A.; Dunietz, B. D.; Dutoi, A. D.; Furlani, T. R.; Gwaltney, S. R.; Heyden, A.; Hirata, S.; Hsu, C. P.; Kedziora, G.; Khalliulin, R. Z.; Klunzinger, P.; Lee, A. M.; Lee, M. S.; Liang, W.; Lotan, I.; Nair, N.; Peters, B.; Proynov, E. I.; Pieniazek, P. A.; Rhee, Y. M.; Ritchie, J.; Rosta, E.; Sherrill, C. D.; Simmonett, A. C.; Subotnik, J. E.; Woodcock, H. L., 3rd; Zhang, W.; Bell, A. T.; Chakraborty, A. K.; Chipman, D. M.; Keil, F. J.; Warshel, A.; Hehre, W. J.; Schaefer, H. F., 3rd; Kong, J.; Krylov, A. I.; Gill, P. M.; Head-Gordon, M. Advances in methods and algorithms in a modern quantum chemistry program package. *Phys. Chem. Chem. Phys.* **2006**, *8* (27), 3172−3191.
(82) Ponder, J. W. *TINKER, Software Tools for Molecular Design*, version 4.2; Washington University School of Medicine: St. Louis, MO, 2004.
(83) Mo, Y.; Subramanian, G.; Gao, J.; Ferguson, D. M. Cation-pi interactions: an energy decomposition analysis and its implication in delta-opioid receptor-ligand binding. *J. Am. Chem. Soc.* **2002**, *124* (17), 4832−4837.

(84) Hong, Y. J.; Tantillo, D. J. C-H center dot center dot center dot pi interactions as modulators of carbocation structure - implications for terpene biosynthesis. *Chem. Sci.* **2013**, *4* (6), 2512−2518.
(85) Wendt, K. U.; Poralla, K.; Schulz, G. E. Structure and function of a squalene cyclase. *Science* **1997**, *277* (5333), 1811−1815.
(86) Mahadevi, A. S.; Sastry, G. N. Cation-pi interaction: its role and relevance in chemistry, biology, and material science. *Chem. Rev.* **2013**, *113* (3), 2100−2138.